International Journal of Modern Physics C
Vol. 20, No. 10 (2009) 1663–1680

World Scientific
www.worldscientific.com

NUMERICAL STUDY OF ASYMMETRIC EFFECT ON A PITCHING FOIL

QING XIAO
Department of Naval Architecture and Marine Engineering
University of Strathclyde, Glasgow, G4 0LZ, UK
qing.xiao@strath.ac.uk

WEI LIAO*
Department of Mathematics and Statistics
Old Dominion University, 4700 Elkhorn Ave
Norfolk, VA 23529, USA
wliao@odu.edu

Received 23 March 2009
Accepted 16 June 2009

This study investigates numerically the effect of asymmetric sinusoidal oscillating motion on the propulsion performance of a pitching foil and attempts to gain insight in whether the low thrust generated by pure pitching could be improved by asymmetric motion. The propulsion performance and flow structure are explored by solving the unsteady Navier–Stokes equations. Computations are conducted for a range of oscillation frequency, pitching amplitude, and asymmetry. The results show that the higher asymmetry can induce the stronger reverse Von Karman vortex in the wake, which in turn leads to the increased thrust. However, the propulsion efficiency reduces as increasing asymmetry. Computed results are further adopted to shed insight into the mechanism of thrust enhancement.

Keywords: Asymmetry; sinusoidal motion; pitching foil; thrust performance.

PACS Nos.: 11.25.Hf, 123.1K.

1. Introduction

The oscillating foil with combined motion of pitching and plunging resembles the wing of flying bird and fin of swimming fish. Biologically inspired, numerous experimental and numerical studies have investigated the flows around an oscillating foil.[1–14,16,19] Previous research has shown that the wake structure downstream of trailing edge plays a significant role on the thrust and lift generation by an oscillating foil. With a low nondimensional oscillating frequency, the wake presents a

*Corresponding author.

classic von Karman vortex street which induces the generation of time-mean drag force. On the other hand, at a higher oscillating frequency, the wake possesses a reverse von Karman vortex street, with the upper row of vortices rotating counterclockwise and the lower row of vortices rotating clockwise. A time-mean thrust force is produced under this condition.

The pure sinusoidal motions of pitching, plunging or combined motions have been extensively examined to study the kinetics and flow characteristics of oscillating foil, such as the lift, thrust, and propulsion efficiency. Typical experimental studies include Anderson *et al.*,[1] Lai and Platzer,[2] Koochesfahani,[3] Read *et al.*,[4] Hover *et al.*,[5] and Lua *et al.*[6] A number of numerical simulations have been conducted by Lewin and Haj-Hariri,[7] Tuncer and Platzer,[8] Young and Lai,[9] Isogai *et al.*,[10] Yang *et al.*,[11] Ramamurti and Sandberg,[12] and Sarkar and Venkatraman.[13,14] The general conclusion from the existing investigations is that the thrust and propulsive efficiency generated by the oscillating foil strongly depend on the various parameters and their combinations, including the amplitudes of pitching and plunging motions, the phase angle difference between these two motions and the nondimensional oscillating frequency.

Although pure sinusoidal motion has been extensively studied, the investigation on different types of pitching/plunging rather than sinusoidal motion is limited. Read *et al.*[4] performed the experiments to investigate the effects of higher-order harmonic plunging motion on the thrust generation and propulsive efficiency of a NACA0012 airfoil undergoing combined plunging and pitching at $\mathrm{Re} = 40\,000$. They found that certain small changes for the harmonic plunging motion can effectively prevent the degradation of effective angle of attack at relatively high frequency. This leads to substantially improved thrust coefficients and nearly constant propulsion efficiency at the high Strouhal numbers.

Subsequently, Hover *et al.*[5] extended the effort of Read *et al.*[4] to the other nonsinusoidal motions. Their trajectory of plunging motion is determined by obtaining the combined effective angle of attack to be a square wave, a symmetric sawtooth wave, and a cosine function rather than a sinusoidal profile. Their experimental results showed that the cosine profile achieves a maximum improvement among the four cases in terms of high thrust force with reasonable high efficiency. Flow visualization results revealed that the improvement of propulsive performance coincides with the partial or complete recovery of a reverse von Karman wake which is associated with the higher thrust force.

Sarkar and Venkatraman[14] performed numerical simulation of the flow over a nonsinusoidal plunging motion over an NACA0012 airfoil using a 2D discrete vortex method. Several nonsinusoidal motions were tested including asymmetric sinusoidal motion, constant heave rate oscillations, and sinusoidal motion with a quiescent gap. They reported that the thrust and propulsion efficiency obtained by the asymmetric sinusoidal motion were higher than those by the pure sinusoidal motion at a given reduced oscillation frequency. However, the constant rate plunging motion did not compare favorably with the harmonic motion.

Coupled motion of plunging and pitching for an oscillating foil has been demonstrated to produce higher thrust efficiently, thus most of previous studies on oscillating foil concentrated on the combined motion. Studies on pure pitching under the incompressible flow condition are very restricted. However, the pure pitching foil has many potential applications in the field of aquatic animal motion such as ostraciiform BCF (body and/or caudal fin locomotion) of fish swimming, which is characterized by the pendulum-like oscillation of caudal fin while the fish body remains basically rigid.[15]

Limited previous research on a pure pitching foil includes Garrick,[16] Koochesfahani,[3] and Sarkar and Venkatraman.[13] The earliest study of Garrick[16] showed that positive thrust force is produced only at relatively high pitching frequency for the pure pitching motion. Koochesfahani[3] performed experiments to study an NACA0012 foil pitching about its quarter-chord point. Detailed wake vortex structure for two pitching amplitudes was investigated. Flow visualization results showed that at a small pitching amplitude, with increasing of oscillating frequency, the wake structure changes from drag producing to thrust producing. The critical frequency of transition from drag to thrust decreases with the pitching amplitude increasing. A different vortex structure was observed for the limited study on an asymmetric pitching motion and no quantitative data of thrust and propulsion efficiency were presented. More recently, Sarkar and Venkatraman[13] studied numerically the pure sinusoidal pitching flow over an NACA0012 airfoil. They found that thrust generation is affected by the pitching parameters such as mean angle of attack, pitching amplitude, oscillating frequency, and pitching axis location.

As seen from above, no attempts have been made to characterize the thrust and efficiency generated for an asymmetric pitching foil. The aim of this study is therefore to investigate numerically the effect of asymmetric sinusoidal oscillating motion on the propulsion performance of a pitching foil to determine whether the low thrust produced by pure pitching could be improved by asymmetric oscillation. The computation will be conducted over a wide range of oscillating frequency, pitching amplitude, and asymmetry. The analysis of computed thrust, input power, propulsion efficiency, pressure distribution, and wake vortex structure is presented to help us better understand the mechanism of the propulsion enhancement caused by the asymmetric sinusoidal motion.

The rest of the paper is organized in the following manner. The computational method adopted is briefly outlined. This is followed by a discussion of numerical results and concluding remarks.

2. Computational Method

2.1. *Governing equations*

In this study, the unsteady viscous flows around an oscillating NACA0012 airfoil are modeled by solving the unsteady Navier–Stokes equations with a compressible solver at low Mach numbers.

The governing equations for unsteady compressible flows are expressed as follows:

$$\frac{\partial}{\partial t}\int_V W dV + \int_S (\boldsymbol{F}_c - \boldsymbol{F}_d)\cdot \boldsymbol{n} dS = 0\,, \tag{1}$$

where V denotes a control volume with closed boundary surface S, and $\boldsymbol{n}$ is the outward unit normal vector on S. The vector $\boldsymbol{W}$ contains the conservative variables.

$$\boldsymbol{W} = (\rho, \rho u, \rho v, \rho w, \rho E)^T\,, \tag{2}$$

where ρ is the density, u, v, and w are the three Cartesian velocity components, and E is the specific total energy of the flow, given by

$$E = e + \frac{1}{2}(u^2 + v^2 + w^2)\,, \tag{3}$$

where e is the internal energy. The flux tensor in Eq. (1) consists of the inviscid convective fluxes $\boldsymbol{F}_c$ and the diffusive fluxes $\boldsymbol{F}_d$. In this study, the arbitrary Lagrangian–Eulerian method is adopted to allow for the moving boundary subject to the oscillating airfoil. It is here achieved by defining fluxes relative to the motion of the control-volume surfaces. Therefore, the convective fluxes $\boldsymbol{F}_c$ are expressed in terms of the relative velocity $\boldsymbol{u} - \boldsymbol{u}_b$, i.e.

$$\boldsymbol{F}_c = \begin{pmatrix} \rho(u-u_b) & \rho(v-v_b) & \rho(w-w_b) \\ \rho u(u-u_b)+p & \rho u(v-v_b) & \rho u(w-w_b) \\ \rho v(u-u_b) & \rho v(v-v_b)+p & \rho v(w-w_b) \\ \rho w(u-u_b) & \rho w(v-v_b) & \rho w(w-w_b)+p \\ \rho H(u-u_b) & \rho H(v-v_b) & \rho H(w-w_b) \end{pmatrix}, \tag{4}$$

where $\boldsymbol{u}_b = (u_b, v_b, w_b)^T$ is the grid velocity vector and $H = E + P/\rho$ is the specific total enthalpy. The diffusive fluxes due to the viscous shear stresses and thermal diffusion can be written as

$$\boldsymbol{F}_d = \begin{pmatrix} 0 & 0 & 0 \\ \tau_{xx} & \tau_{xy} & \tau_{xz} \\ \tau_{yx} & \tau_{yy} & \tau_{yz} \\ \tau_{zx} & \tau_{zy} & \tau_{zz} \\ \theta_x & \theta_y & \theta_z \end{pmatrix}. \tag{5}$$

Here $\tau_{\alpha\beta}$, with α, $\beta \in (x, y, z)$ is the stress tensor and

$$\theta_x = u\tau_{xx} + v\tau_{xy} + w\tau_{xz} - q_x\,,$$
$$\theta_y = u\tau_{xy} + v\tau_{yy} + w\tau_{zy} - q_y\,,$$
$$\theta_z = u\tau_{xz} + v\tau_{yz} + w\tau_{zz} - q_z\,.$$

In a Newton–Fourier fluid, the viscous shear stresses and heat fluxes can be defined as

$$\tau_{\alpha\beta} = (\partial_\alpha u_\beta + \partial_\beta u_\alpha) - \frac{2}{3}\delta_{\alpha\beta}\partial_\alpha u_\beta \,,$$

$$q_\alpha = -k\partial_\alpha \Theta \,,$$

with the dynamic viscosity μ, the thermal conductivity k, and the temperature Θ. The coefficient of laminar viscosity is obtained by the Sutherlands formula,

$$\frac{\mu}{\mu_{\text{ref}}} = \frac{\Theta_{\text{ref}} + 110.3}{\Theta + 110.3}\left(\frac{\Theta}{\Theta_{\text{ref}}}\right)^{3/2} , \tag{6}$$

where Θ_{ref} and μ_{ref} are the absolute temperature and dynamic viscosity at reference with $\Theta_{\text{ref}} = 273$ K.

2.2. *Numerical methods*

The basic numerical method used to solve the above system of equations in this paper follows that described in detail by Xiao *et al.*[17,18] A central-difference scheme with a blend of second- and fourth-order artificial dissipation is used with dual timestepping method for unsteady problems. Parallelism is achieved through the implementation of MPI (message passing interface) protocol. The computational domain is decomposed into structured subdivisions. Each block is considered as a single entity, only flow quantities at the block boundaries need to be exchanged. An explicit five-stage Runge–Kutta type scheme is used to solve the discretized equations. The multigrid method is adopted to accelerate the convergence of the solution.

2.3. *Quantities related with asymmetric pitching motions of foils*

The asymmetric sinusoidal motion of a pitching foil is expressed as[14]:

$$\theta(t) = \begin{cases} \theta_0 \sin\left(\dfrac{\omega t}{2s} - \dfrac{\pi}{2}\right) & 0 \le t \le sT \\ \theta_0 \sin\left(\dfrac{\omega(T-t)}{2(1-s)} + \dfrac{\pi}{2}\right) & sT \le t \le T \end{cases} , \tag{7}$$

where T is the oscillating period, ω is the angular frequency, θ_0 is the pitching amplitude, and s is the asymmetry with symmetric pitching represented by $s = 0.5$.

For an oscillating foil, the propulsion efficiency η is defined as

$$\eta = \frac{C_t}{C_{\text{ip}}} \,, \tag{8}$$

where C_t is the mean thrust coefficient during one oscillation period and C_{ip} is the mean input power coefficient. The thrust coefficient C_t is defined as

$$C_t = \frac{\bar{F}}{(1/2)\rho U_\infty^2 c} \,, \tag{9}$$

where c is the chord length of the foil, $\bar{F}$ is the time-averaged value of the force component $X(t)$ in the x direction and is given by

$$\bar{F} = \frac{1}{T}\int_0^T X(t)dt\,. \tag{10}$$

The power coefficient $C_{\rm ip}$ can be calculated by

$$C_{\rm ip} = \frac{\bar{P}}{(1/2)\rho U_\infty^3 c} \tag{11}$$

with

$$\bar{P} = \frac{1}{T}\left[\int_0^T Y(t)\frac{dh(t)}{dt}dt + \int_0^T M(t)\frac{d\theta(t)}{dt}dt\right], \tag{12}$$

where $Y(t)$ is the force component in y direction and $M(t)$ is the pitching moment. The pressure coefficient C_p is defined as

$$C_p = \frac{p - p_\infty}{(1/2)\rho U_\infty^2}\,. \tag{13}$$

The Reynolds number Re used in the current work is defined by $\mathrm{Re} = U_\infty c/\nu$, where U_∞ is the free-stream velocity and ν is the kinematic viscosity. Pitching axis is located at one-quarter of chamber. Computations are conducted for different oscillation reduced frequencies $k(k = \omega c/2U_\infty = fc\pi/U_\infty)$ varying from 3 to 14, three different pitching amplitudes, $\theta_0 = 2$, 4, and 6° and a series of asymmetries $s = 0.3$, 0.4 and 0.5.

3. Results and Discussions

3.1. *Code validation and mesh dependence test*

The capability of the present code for calculating unsteady compressible viscous flows have been extensively examined in Xiao *et al.*[17,18] The validation of this code for modeling near incompressible flows over an oscillating foil with coupled plunging and pitching motions at low free-stream Mach numbers was performed by Xiao and Liao.[19] Test cases on the flows over a symmetric pitching airfoil are conducted here prior to the present detailed investigation. Comparison with the available experimental and computational data from Koochesfahani[3] and Ramamurti and Sandberg[12] is carried out. The Reynolds number investigated is around $\mathrm{Re} = 10^4$ and therefore the laminar flow is assumed.

The mesh for the present computation is a C-mesh, which extends 20 chords length in all directions. Three sets of meshes with the sizes of 193×33, 385×65, and 513×129 are investigated herein for grid independence test. Comparison of the three results on instant drag coefficient and power coefficient variations with iteration time for $\theta_0 = 4°$ and $k = 9$ only shows negligible differences between the solutions on the 385×65 grid and those on the 513×129 grid. Therefore, the

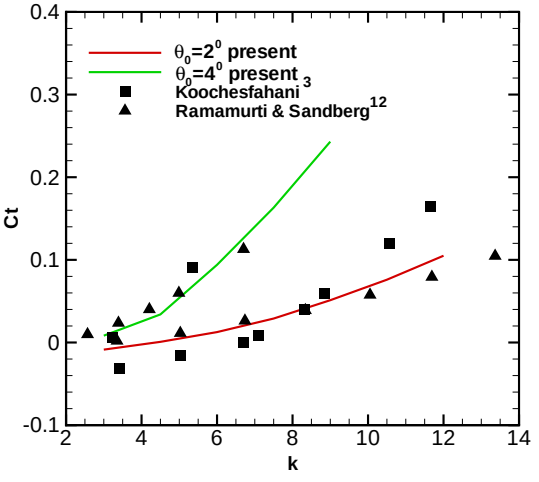

Fig. 1. Thrust coefficient variation with reduced frequency in comparison with the existing experiments and computations for the symmetric motion.

computational results presented in the following are conducted on the grid 385×65 unless otherwise stated.

Figure 1 shows the computed time-mean thrust coefficient variation with k as well as experimental data of Koochesfahani[3] and computational results of Ramamurti and Sandberg[12] given that pitching amplitudes are equal to $\theta_0 = 2°$ and $\theta_0 = 4°$. Computation of Ramamurti and Sandberg[12] is based on the incompressible method, while for the present modeling, compressible code is adopted with the far-stream Mach number being 0.05. As seen from the figure, both the computation and experiment exhibit the increased thrust coefficient with increasing k. For a given reduced frequency, thrust force significantly increases with the pitching amplitude θ_0. The current simulations are closely in agreement with previous results of Ramamurti and Sandberg[12] and Koochesfahani[3] for two pitching amplitudes tested here. Therefore, the present code shows the good capability for simulating incompressible flows over an oscillating foil. Hence, all computations in the following study are conducted at the far-stream Mach number Ma = 0.05.

3.2. *Results for symmetric sinusoidal motion*

The symmetric sinusoidal motion is first investigated here as a special asymmetric case with the asymmetric ratio $s = 0.5$. In Figs. 2(a)–2(c), the results are shown for time-mean thrust coefficient, input power coefficient, and propulsion efficiency. As seen from Fig. 2(a), for a given θ_0, thrust coefficient monotonically increases with k. The same trend can be observed in Fig. 2(b) for mean power coefficient. Figures 2(a) and 2(b) also illustrate that, as the pitching amplitude θ_0 increases, with a fixed k, both thrust and power coefficients increase and thus $\theta_0 = 6°$ always has the largest C_t and C_{ip} among the three tested pitching amplitudes. With $\theta_0 = 2°$, the flow

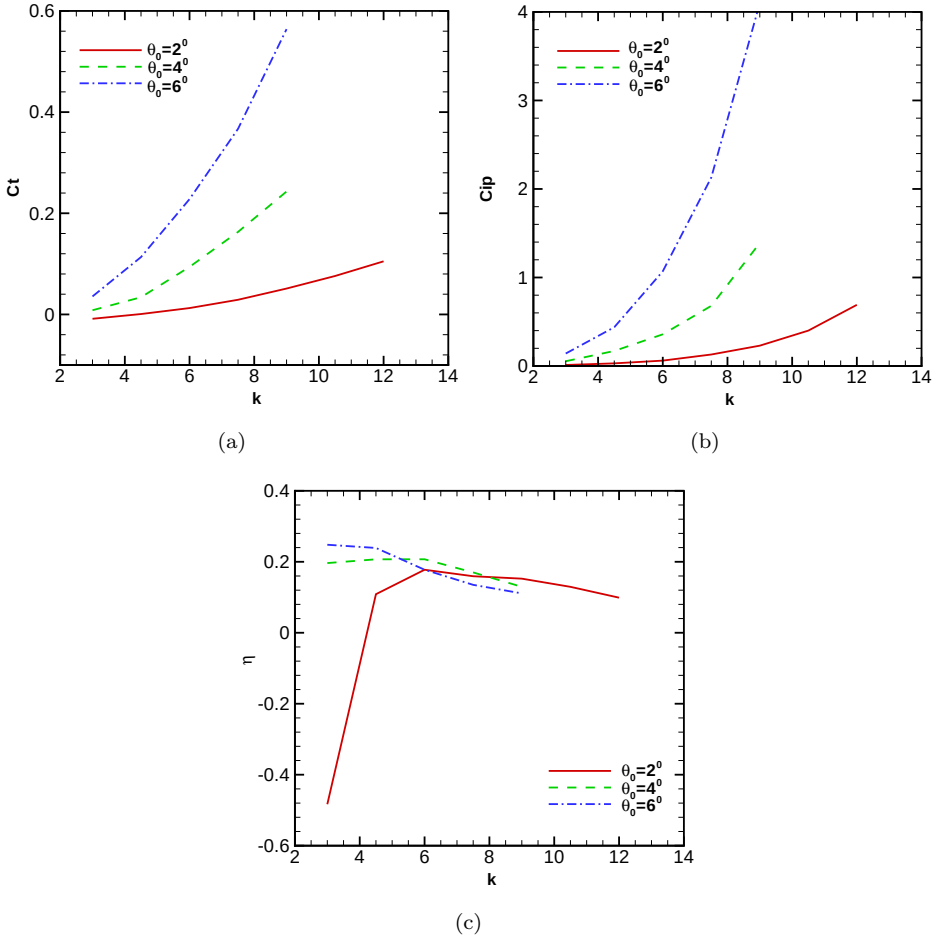

Fig. 2. (a) Mean thrust coefficient, (b) power coefficient, and (c) propulsion efficiency variation with k for the symmetric case ($s = 0.5$).

changes from drag producing to thrust producing around $k = 5$ which is indicated by the sign change of C_t. For larger pitching amplitudes like $\theta_0 = 4°$ and $\theta_0 = 6°$, the flows always present the thrust producing within the tested k range.

The propulsion efficiency vs k for two larger pitching amplitudes $\theta_0 = 4°$ and $\theta_0 = 6°$, shown in Fig. 2(c), illustrates that η initially presents a flat distribution until about $k = 5$, indicating the equally increasing of thrust force and input power. As k increases, η starts decaying suggesting the faster increasing of input power than that of thrust force. For $\theta_0 = 2°$, η increases with k when $k < 6$ and thereafter decreases with further increasing of k. As seen from Figs. 2(a) and 2(b), although both C_t and C_{ip} increase with k, generally the slope of C_{ip} vs k is larger than that of C_t at a given k, which causes η to decrease as k increases to higher values.

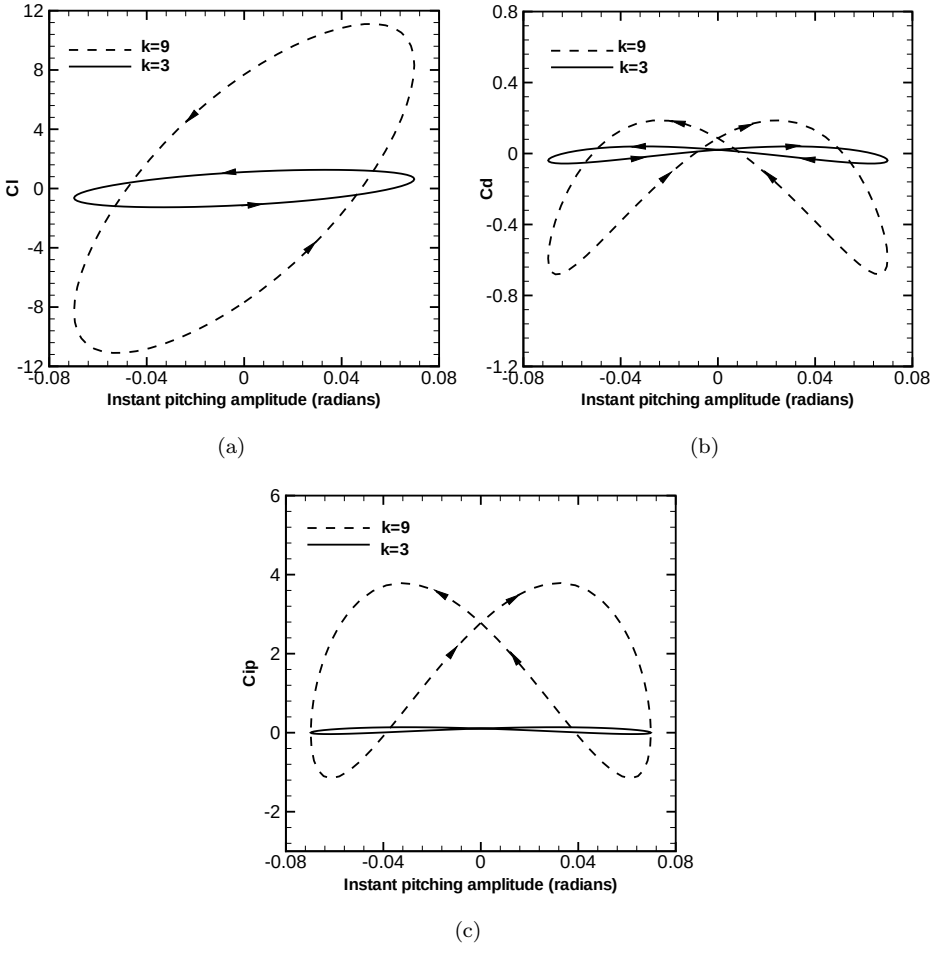

Fig. 3. Effect of oscillation frequency on (a) instant lift coefficient, (b) drag coefficient, and (c) power coefficient, variation with pitching amplitude in one cycle for the symmetric motion ($s = 0.5$, $\theta_0 = 4°$, $k = 9$ and 3).

The typical variations of instant lift coefficient C_l, drag coefficient C_d $(= -C_t)$, and power coefficient C_{ip} with instant pitching amplitude $\theta(t)$ are shown in Figs. 3(a)–3(c) for $k = 3$ and $k = 9$ with same pitching amplitude $\theta_0 = 4°$. The corresponding time history of $\theta(t)$, C_l, C_t, and C_{ip} are shown in Fig. 4. As seen from Figs. 3(a) and 4(b), for both cases, the lift coefficients C_l in the down-stroke motion have higher values than those in the up-stroke motion and the amplitude of C_l for $k = 9$ is much larger than that for $k = 3$. Both C_l vary at the same frequency in spite of different frequencies with $k = 3$ and $k = 9$ for the pitching motions. However, there is phase shift between C_l vs t/T and the corresponding pitching motion in both cases. The drag coefficient and power coefficient in Figs. 3(b)–3(c) and 4(c)–4(d), however, show that C_d and C_{ip} vary with time at twice the fre-

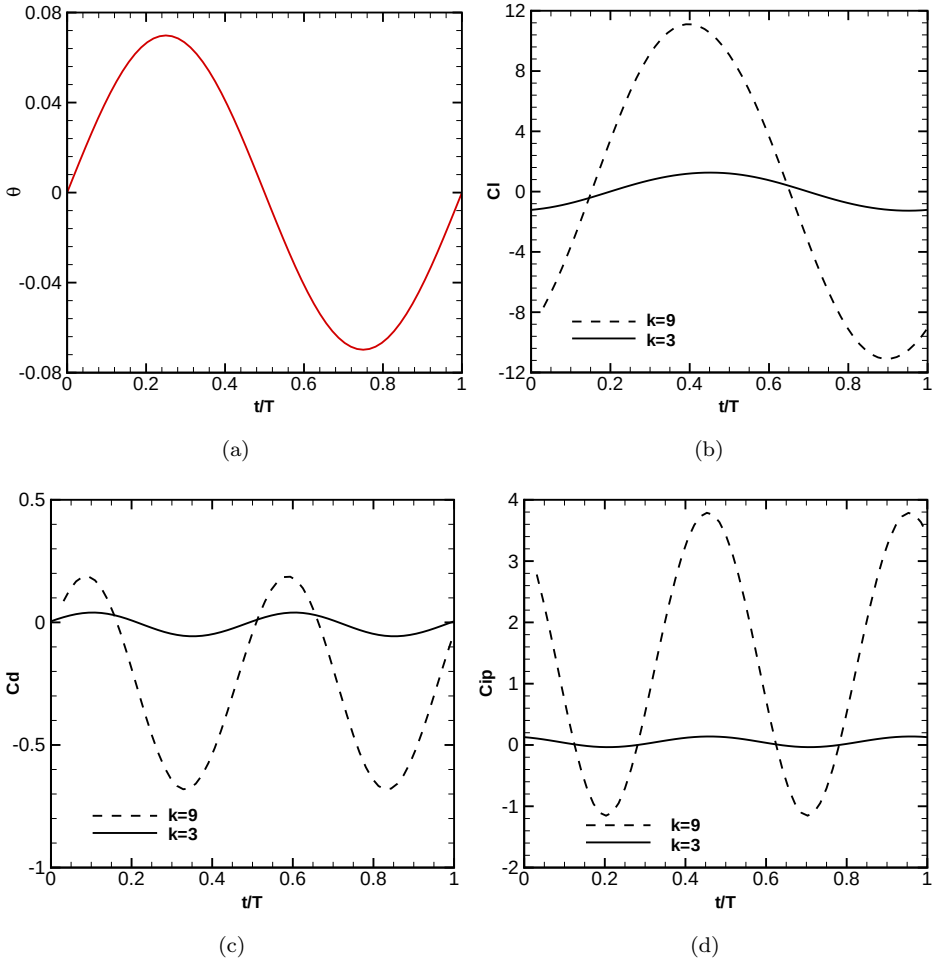

Fig. 4. Effect of oscillation frequency on (a) instant pitching amplitude, (b) lift coefficient, (c) drag coefficient, and (d) power coefficient, variation with time in one cycle for the symmetric motion ($s = 0.5$, $\theta_0 = 4°$, $k = 9$ and 3).

quency as the pitching motion. The variations of C_t and C_{ip} vs pitching angle are symmetric during the down-stroke and up-stroke motion. The impact of different oscillation frequency on propulsion performance is clearly reflected in the figures. With $k = 9$, the oscillation amplitudes of C_t and C_{ip} are much larger than those with $k = 3$, which results in the increased time-mean thrust coefficient and power coefficient with increasing k as shown in Figs. 2(a) and 2(b).

The effect of the pitching amplitude θ_0 on time history of instant pitching amplitude, lift coefficient, drag coefficient, and propulsion coefficient are shown in Figs. 5(a)–5(d) for three amplitudes $\theta_0 = 2°$, $\theta_0 = 4°$, and $\theta_0 = 6°$ with the same frequency of $k = 6$. Compared to Fig. 4, it can be seen that with a fixed k, increasing amplitude has the analogous effect on the variation of C_l, C_t, and C_{ip} as

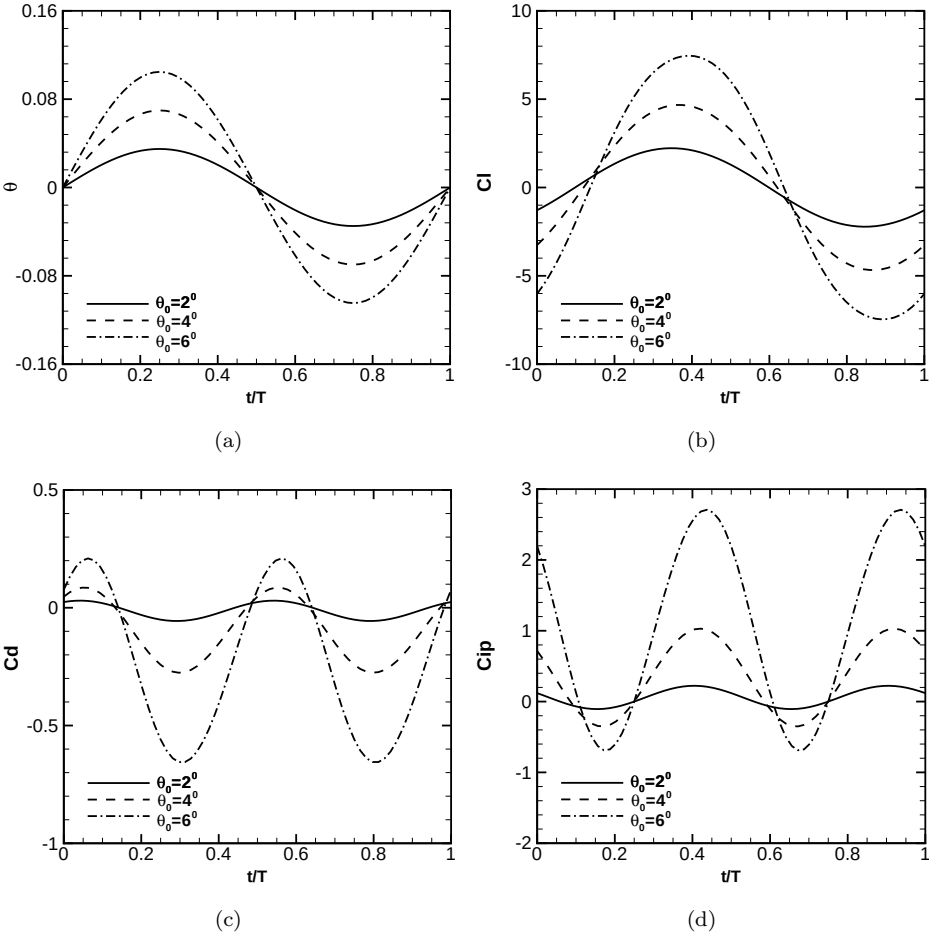

Fig. 5. Effect of the pitching amplitude θ_0 on (a) instant pitching amplitude, (b) lift coefficient, (c) drag coefficient, and (d) power coefficient, variation with time in one oscillation cycle for the symmetric motion ($s = 0.5$, $k = 6$, and $\theta_0 = 2$, 4, 6°).

k increases given θ_0 remaining constant. In other words, instant thrust coefficient and power coefficient increase with θ_0 at a given k resulting in the time-mean C_t and C_{ip} enhancement as indicated in Figs. 2(a) and 2(b).

Figure 6 shows the typical results for the vorticity contours with symmetric pitching motion for $k = 9$ and $\theta_0 = 6°$. Due to the symmetry, plots are only shown for half an oscillating cycle. Clearly indicated in the figure, the wake structure at this flow condition represents the vortex street featuring thrust generation, i.e. the upper row vortex rotates counterclockwise (red) and the lower vortex rotates clockwise (blue).

To summarize, within the parameters investigated for symmetric pitching motion, the flow is shown to be thrust generation. The time-mean thrust and input

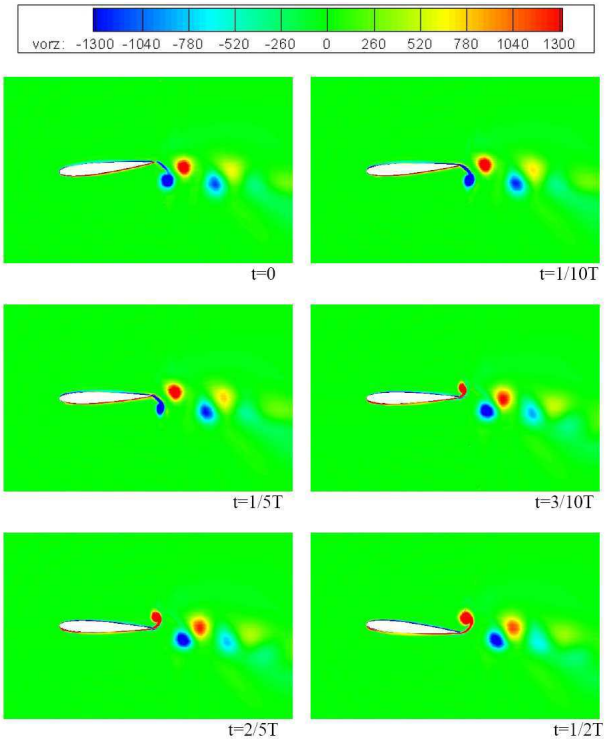

Fig. 6. (Color online) Vorticity contours for the symmetric pitching with $k = 9$ and $\theta_0 = 6°$ (red: counter clockwise; blue: clockwise).

power required for oscillation increase with k at a given pitching amplitude, and hence the propulsion efficiency keeps almost constant before it decreases with k. This is in close agreement with the previous findings of computation (Sarkar and Venkatraman[13]) and experiment (Koochesfahani[3]).

3.3. *Results for asymmetric sinusoidal motion*

In this part, the effect of asymmetric pitching motion, with s deviating from 0.5, on the propulsion of an oscillating foil will be discussed. The effect of asymmetry on the time-mean thrust coefficient, power coefficient, and propulsion efficiency is summarized in Figs. 7(a)–7(c) for two pitching amplitudes $\theta_0 = 2°$ and $\theta_0 = 6°$, respectively. Note that results for $\theta_0 = 4°$ are omitted here for space limitation as the trends are similar to those of $\theta_0 = 2°$.

As seen from Fig. 7(a), for two θ_0 shown here, thrust coefficient increases with asymmetry at a given oscillation frequency. Similar trend is found for the input power coefficient presented in Fig. 7(b). Compared with curve C_t vs k, asymmetric effect on C_{ip} vs k is more profound, i.e. the increasing of C_{ip} with higher asymmetry is much larger than that of C_t at a fixed k. As a consequence, the

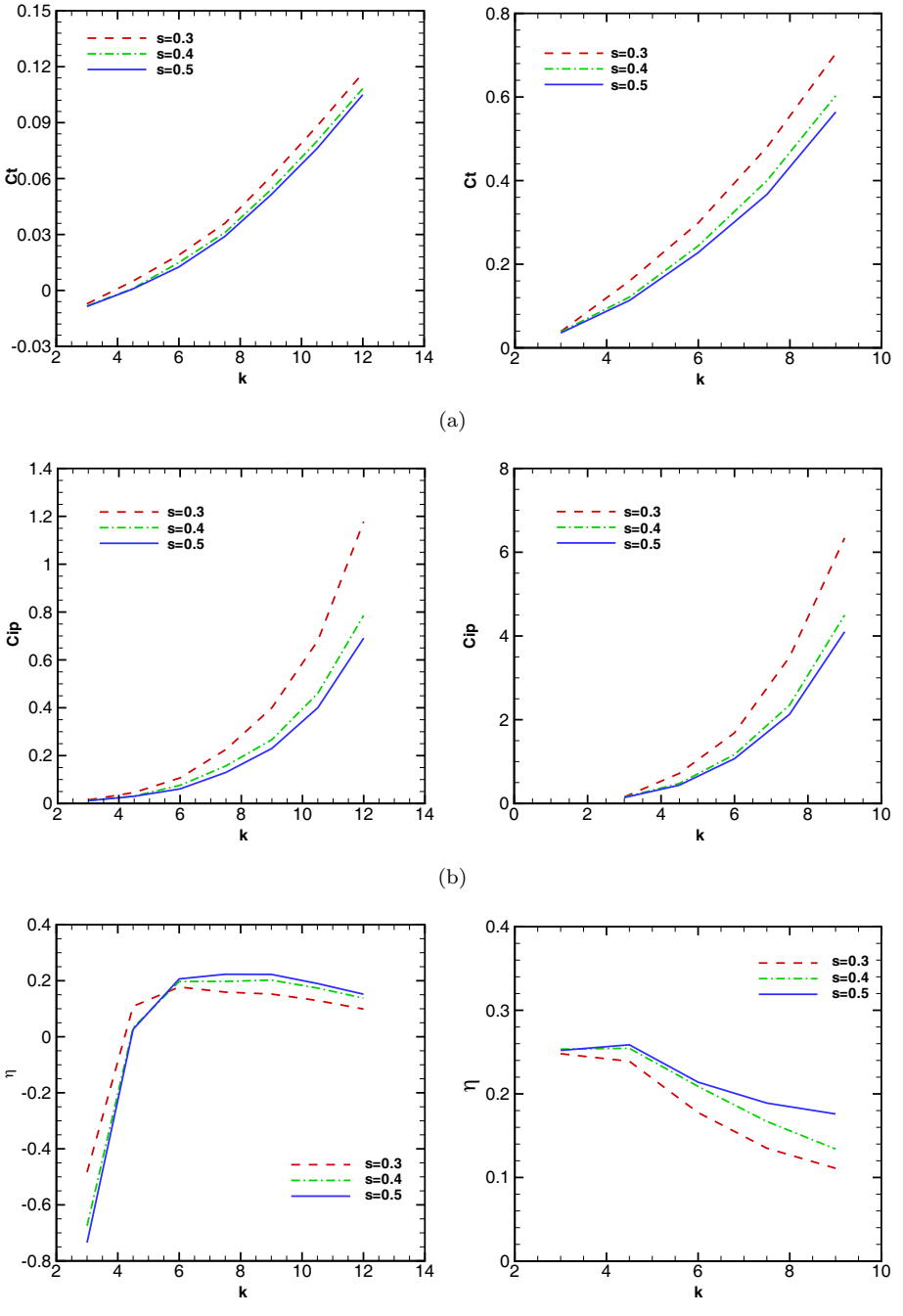

Fig. 7. (a) Mean thrust coefficient, (b) power coefficient, and (c) propulsion efficiency, variation with k. Left column: $\theta_0 = 2°$; right column: $\theta_0 = 6°$.

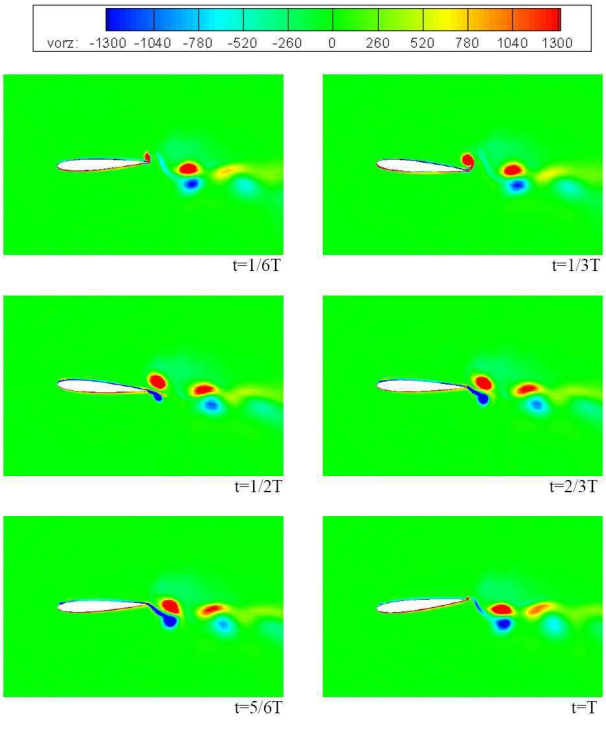

Fig. 8. (Color online) Vorticity contours for the asymmetric pitching with $s = 0.3$, $k = 9$, and $\theta_0 = 6°$ (red: counterclockwise; blue: clockwise).

propulsion efficiency, which is a ratio of thrust coefficient to input power coefficient, decays with asymmetry at a given k for both pitching amplitudes. This is more apparent for the case $\theta_0 = 6°$ as displayed in Fig. 7(c).

The vortex contour plots for an asymmetric case with $s = 0.3$, $k = 9$, and $\theta_0 = 6°$ are shown in Fig. 8. Compared to the symmetric case in Fig. 6, the general wake structure is similar with typical features of the reverse Karman vortex. At most time instants shown in the figures, two large counterclockwise rotating vortices appear on the upper row, and two small clockwise rotating vortices occur on the lower row. The vortices for the asymmetric case are generally more vigorous than those for the corresponding symmetric case especially during the fast acceleration time interval. We believe this is the reason that asymmetry can enhance the thrust performance.

The asymmetry effect on the instant lift coefficient, drag coefficient, and power coefficient vs $\theta(t)$ is shown in Figs. 9(a)–9(c) for $s = 0.3$, 0.4, and 0.5 with $\theta_0 = 4°$ at $k = 9$ and $k = 3$, respectively. In comparison with the symmetric case at $s = 0.5$, lift coefficient with asymmetric pitching motion presents the asymmetric distribution during the up-stroke and down-stroke. This induces the time-mean nonzero C_l with its value increasing with asymmetry. This asymmetry feature is also revealed by the drag coefficient distribution shown in Fig. 9(b). The instant

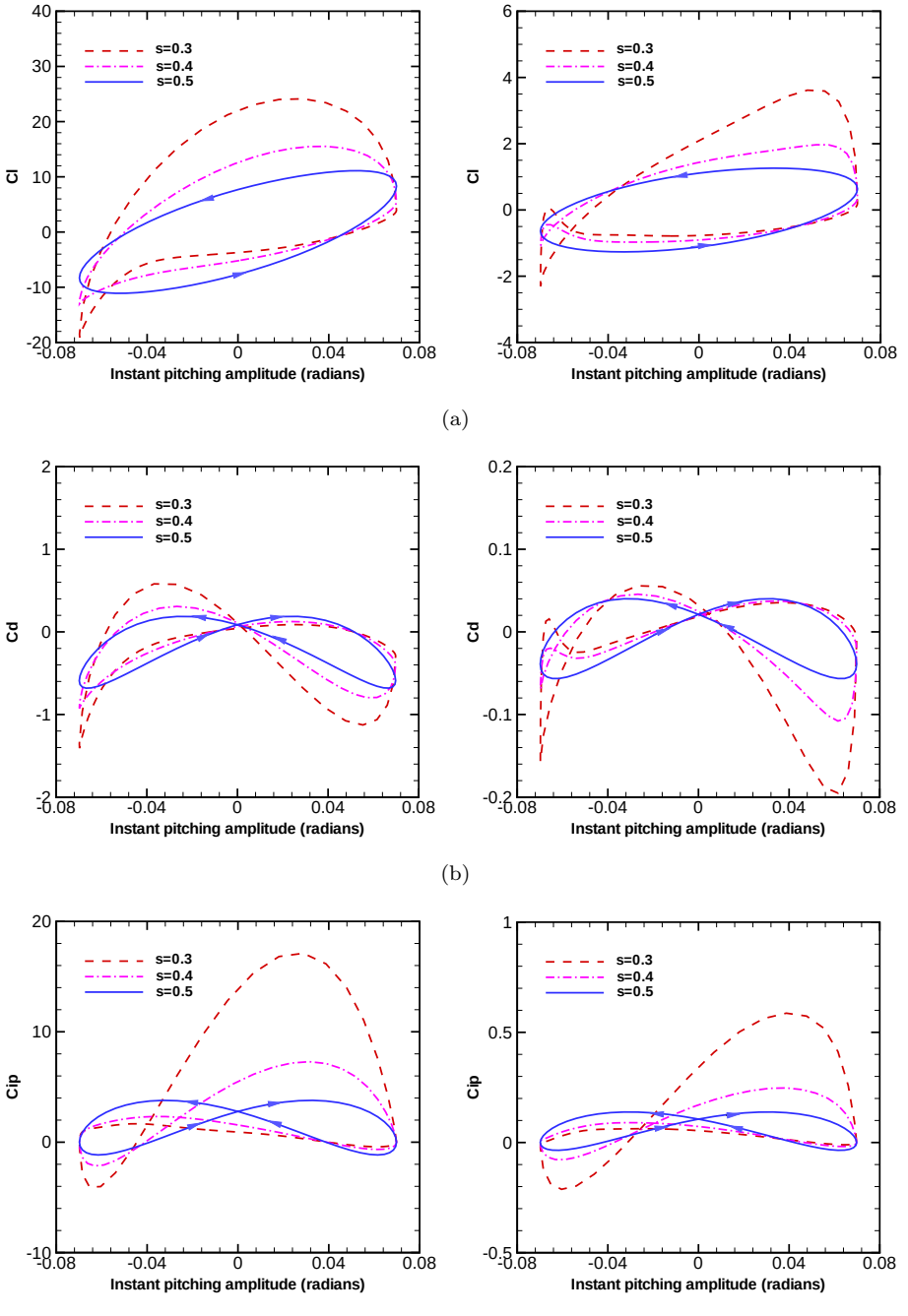

Fig. 9. Asymmetry effect on (a) instant lift coefficient, (b) drag coefficient, and (c) power coefficient, variation with pitching amplitude in one oscillation cycle for the asymmetric sinusoidal motions at $\theta_0 = 4°$. Left column: $k = 9$; right column: $k = 3$.

minimum C_d (or maximum C_t) with $s = 0.3$ and 0.4 is higher than that with $s = 0.5$, which implies the increasing of time-mean thrust with asymmetric pitching motion as shown in Fig. 7. Power coefficient profiles displayed in Fig. 9(c) also present a significant asymmetry of $C_{\rm ip}$ vs $\theta(t)$. At the same time, Fig. 9 demonstrates the similar trend of asymmetry for both frequencies $k = 9$ and $k = 3$. With the lower frequency $k = 3$, however, the curves of C_l vs $\theta(t)$ and C_d vs $\theta(t)$ change from one loop with $k = 9$ to two loops and two loops with $k = 9$ to three loops, respectively.

To better understand the time interval during which the asymmetric influence is the most apparent in one oscillation period, we plotted the time history of $\theta(t)$, $C_l(t)$, $C_d(t)$, and $C_{\rm ip}(t)$ with $\theta_0 = 4^\circ$ in Figs. 10 and 11 for $k = 9$ and 3, respectively.

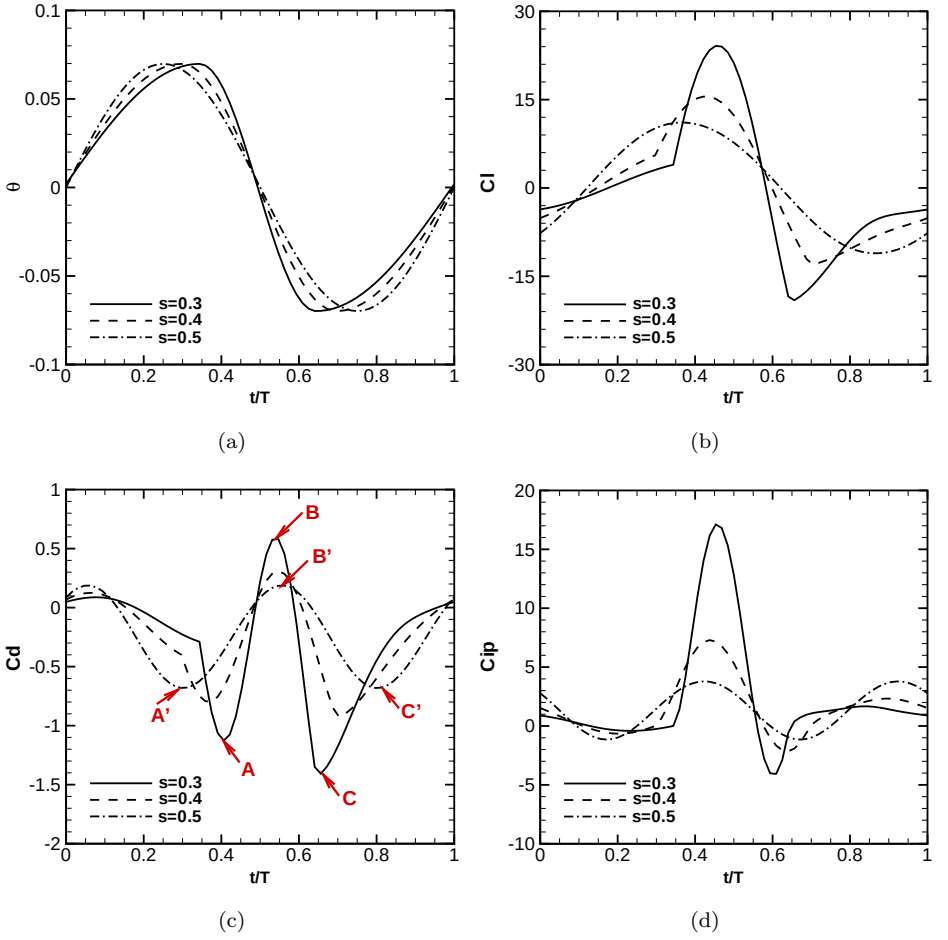

Fig. 10. (a) Instant pitching amplitude, (b) lift coefficient, (c) drag coefficient, and (d) power coefficient, variation with time in one oscillation cycle for the asymmetric sinusoidal motions at $\theta_0 = 4^\circ$ and $k = 9$.

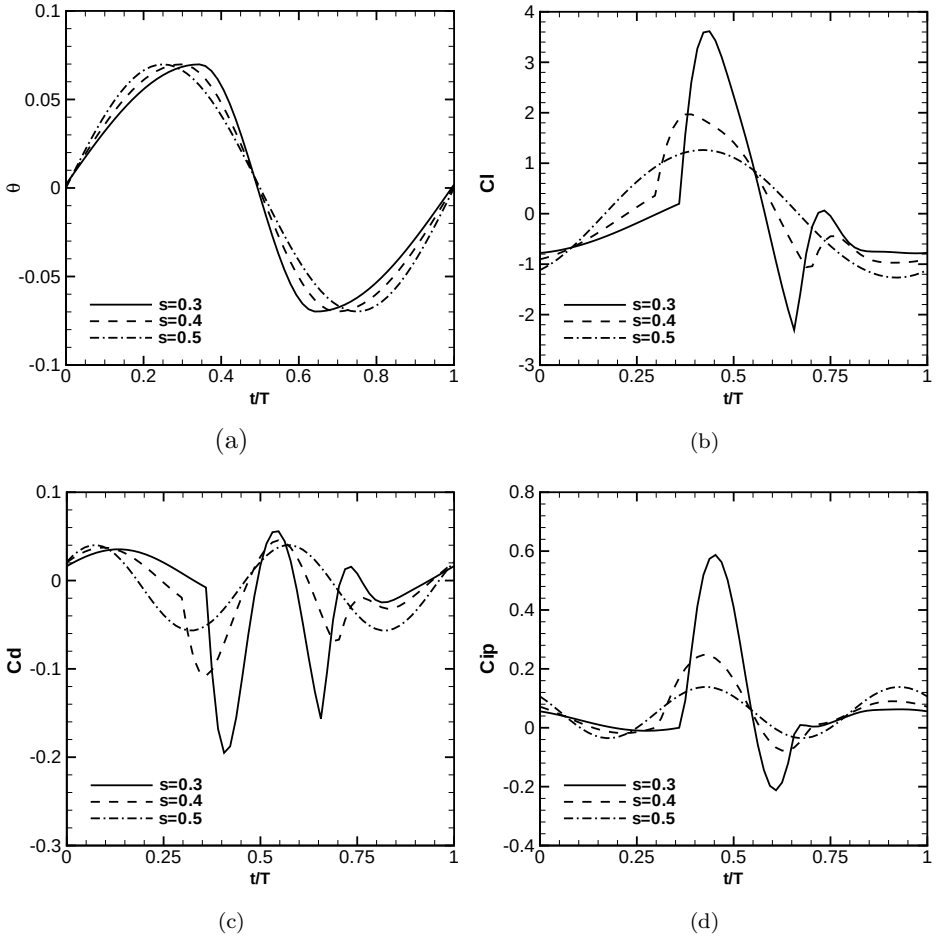

Fig. 11. (a) Instant pitching amplitude, (b) lift coefficient, (c) drag coefficient, and (d) power coefficient variation with time in one oscillation cycle for the asymmetric sinusoidal motions at $\theta_0 = 4^\circ$ and $k = 3$.

As asymmetry increases, noticeable variations are clearly seen for C_l, C_d, and C_{ip} distributions in the phase of fast acceleration (from $+\theta_{\max}$ to $-\theta_{\max}$). For lift coefficient shown in Figs. 10(b) and 11(b), the peak values of C_l with $s = 0.3$ are about two and three times those of $s = 0.5$ for $k = 9$ and 3, respectively. Given $s = 0.3$, three peak values of C_d occur at time instants around $t/T = 0.4$, 0.55, and 0.65 (indicated by A, B, and C) as revealed in Fig. 10(c). Compared to the corresponding peak values in the symmetric case marked by A′, B′, and C′, the peak thrust at $s = 0.3$ is around twice as high as that at $s = 0.5$. Similar trend is observed in Fig. 11(c) for $k = 3$ although the amplitudes of all curves are much smaller than those in Fig. 10(c).

4. Conclusion

In this paper, the numerical computation has been conducted on investigating the effect of asymmetric pitching motion on the propulsion performance of an oscillating NACA0012 hydrofoil. The simulation is conducted by solving the unsteady Navier–Stokes equation for a wide range of oscillation frequency, three different pitching amplitudes, and a series of asymmetry.

For both symmetric and asymmetric sinusoidal pitching, thrust coefficient and input power coefficient increase with oscillating frequency at a given pitching amplitude. The propulsion efficiency, however, remains relatively constant before slightly decaying with frequency. Larger pitching amplitude results in the generation of higher thrust and power, but has minor effect on the efficiency.

Significant improvement on thrust coefficient has been achieved if the pitching becomes asymmetric. Meanwhile, the input power coefficient increases faster than thrust coefficient at a fixed frequency leading to the reduction of propulsion efficiency. Examination of instant thrust coefficient and vortex contour in the fast acceleration time interval reveals the stronger reverse Karman vortex wake at larger asymmetry like $s = 0.3$ than that in the symmetric case with $s = 0.5$. This is believed to cause the enhancement of thrust in the asymmetric cases. The present computational results suggest that asymmetric sinusoidal motion could be a valuable tool in achieving better thrust performance when a hydrofoil only undergoes a pure pitching motion.

References

1. J. M. Anderson, K. Streitlien, D. S. Barrett and M. S. Triantafyllou, *J. Fluid. Mech.* **360**, 41 (1998).
2. J. C. S. Lai and M. F. Platzer, *AIAA J.* **37**, 1529 (1999).
3. M. M. Koochesfahani, *AIAA J.* **27**, 1200 (1989).
4. D. A. Read, F. S. Hover and M. S. Triantafyllou, *J. Fluid. Struct.* **17**, 163 (2003).
5. F. S. Hover, O. Haugsdal and M. S. Triantafyllou, *J. Fluid. Struct.* **19**, 37 (2004).
6. K. B. Lua, T. T. Lim and K. S. Yeo, *AIAA J.* **45** (2007).
7. G. C. Lewin and H. Haj-hariri, *J. Fluid. Mech.* **492**, 339 (2003).
8. I. H. Tuncer and M. F. Platzer, *J. Aircraft.* **37**, 514 (2000).
9. J. Young and J. C. S. Lai, *AIAA J.* **42**, 2042 (2004).
10. K. Isogai, Y. Shinmoto and Y. Watanabe, *AIAA J.* **37**, 1145 (1999).
11. S. Yang, S. Luo, F. Liu and H.-M. Tsai, *AIAA-2005-1404* (2005).
12. R. Ramamurti and W. Sandberg, *AIAA J.* **39**, 253 (2001).
13. S. Sarkar and K. Venkatraman, *Comp. Fluids* **35**, 16 (2006).
14. S. Sarkar and K. Venkatraman, *Int. J. Numer. Meth. Fluids* **51**, 1 (2006).
15. M. Sfakiotakis, D. M. Lane, J. Bruce and C. Davies, *IEEE J. Ocean. Eng.* **34**, 237 (1999).
16. I. E. Garrick, *NACA 567* (1937).
17. Q. Xiao, H.-M. Tsai and D. Papamoschou, *AIAA J.* **45**, 532 (2007).
18. Q. Xiao, H.-M. Tsai and F. Liu, *AIAA J.* **44**, 620 (2006).
19. Q. Xiao and W. Liao, *AIAA-2009-725* (2009).